photonics

MDPI

Article

Stable, Tunable High-Repetition-Rate Operation of Gain-Switched Semiconductor Laser via Hybrid Current-Pulse-Width Control

Jinxu Fang [1,2], Yanyan Qi [2], Yan Liang [1,2,*] and Heping Zeng [1,3]

[1] Shanghai Research Center for Quantum Sciences, Shanghai 201315, China; 243350576@st.usst.edu.cn (J.F.); hpzeng@phy.ecnu.edu.cn (H.Z.)
[2] School of Optical-Electrical and Computer Engineering, University of Shanghai for Science and Technology, Shanghai 200093, China; 255340591@st.usst.edu.cn
[3] State Key Laboratory of Precision Spectroscopy, East China Normal University, Shanghai 200062, China
* Correspondence: yanliang@usst.edu.cn

Abstract

The phenomenon of pulse tailing, primarily caused by relaxation oscillations, presents a significant challenge to increasing the repetition rates of gain-switched semiconductor lasers. This paper proposes a novel approach to mitigate this issue by simultaneously regulating both the magnitude and pulse width of the pump current, enabling stable, tail-free pulse generation across a broad range of repetition frequencies. Numerical solutions to the carrier rate equations are first employed to investigate the origins of optical pulse tailing. By reducing the current injection duration from 200 ps to 50 ps, carrier injection is effectively truncated, suppressing relaxation oscillations. However, this reduction also leads to a decrease in peak optical pulse power, limiting the laser's applicability. Increasing the injection current's magnitude provides a solution. Consequently, a high-precision circuit design has been developed to digitally adjust both the magnitude with a precision of ~3 μA and the pulse width with a resolution of 5 ps. This configuration successfully generates 200 ps optical pulses with a single-pulse energy of 0.96 pJ at 1550 nm, over a repetition rate range from 10 kHz to 1 GHz. With this laser as the transmitter, RZ-OOK modulated signal transmission at a slot rate of 250 MHz has been realized. The proposed scheme offers a stable, reliable optical emission source, making it ideal for high-speed, high-capacity optical time-division multiplexing communication, time-resolved spectroscopy, and laser ranging and imaging applications.

Keywords: gain-switched laser diode; pulse tailing elimination; rate equations; carrier and photon density; pulse control

Check for updates

Received: 28 April 2026
Revised: 21 May 2026
Accepted: 27 May 2026
Published: 30 May 2026

Copyright: © 2026 by the authors. Licensee MDPI, Basel, Switzerland. This article is an open access article distributed under the terms and conditions of the Creative Commons Attribution (CC BY) license.

1. Introduction

Gain-switched semiconductor lasers feature a simple structure, high operational stability, and flexible control of repetition rate and pulse width, which has led to their widespread use in quantum communication, LiDAR, and time-resolved spectroscopy [1–4]. Their capability to generate high-repetition-rate pulses with low timing jitter, together with high energy efficiency and low cost, further makes them indispensable for applications in medical imaging, environmental monitoring, and precision metrology [5–7]. However, as the repetition rate increases, significant pulse tailing phenomena emerge, severely compromising the stability of the output pulses. In optical communication systems, this

would result in strong interference between adjacent channels, degrading transmission performance and potentially causing communication interruptions [8,9].

In gain-switched semiconductor lasers, optical pulse generation is a modulation process driven by the transient dynamics of charge carriers and photons [10]. A periodic pump current raises the carrier density above the threshold Nth, generating a sharp optical pulse via stimulated emission. If the pump current is not promptly terminated after rapid carrier depletion, carriers reaccumulate and induce relaxation oscillations, leading to secondary peaks or a slowly decaying trailing edge after the main pulse, commonly referred to as pulse tailing [11,12]. Thus far, various methods have been proposed to suppress relaxation oscillation and eliminate pulse tails. Yang et al. introduced self-injection feedback in erbium-doped fiber lasers, reducing relaxation oscillation noise by up to 18.08 dB [13]. Wada et al. used a fiber Sagnac interferometer as an external pulse shaper to filter unwanted spectral components and pulse tails from multimode laser diodes [14]. However, such optical systems are often complex and sensitive to environmental disturbances. Li et al. proposed a step-pulse modulation technique with a two-step driving current (pre-bias and main injection) to smooth population inversion buildup, suppress pulse ringing, and generate short pulses with more symmetric waveforms and higher peak power [15]. Recently, Zhang et al. reported an all-electrical smoothing strategy using optimized driving signals to precisely control carrier–photon dynamics, eliminating multiple spikes in gain-switching operation [16]. Nevertheless, this approach requires picosecond-level waveform accuracy at high repetition rates, limiting its practicality for low-cost and large-scale applications. We summarized the properties of the proposed solutions, listed in Table 1.

Table 1. Comparison of properties of proposed solutions to suppress pulse tailing.

Methods	Type	Wavelength	Repetition Rate	Pulse Width
Optical Sagnac Loop [14]	Optical	1540 nm	Fixed (@ 1 GHz)	20 ps
Step-Pulse Modulation [15]	Electrical	1550 nm	/	24~36 ps
Electrically Smoothing [16]	Electrical	1270 nm	/	~100 ps
Hybrid Digital Control (This work)	Electrical	1550 nm	10 kHz–1 GHz	~200 ps

In this paper, we propose a high-precision driving circuit, which is capable of digitally adjusting both the magnitude with a precision of ~3 μA and the pulse width with a resolution of 5 ps, to bias a commercially available DFB laser at 1550 nm. A numerical simulation model based on carrier rate equations is employed to provide a theoretical basis for the design of the driving circuit. The simulation investigates the transient responses under Gaussian pumping waveforms with different repetition frequencies, and explores the mechanism by which reducing the electrical pulse width effectively suppresses optical pulse tailing. Through precise adjustment of the pump current's DC bias and pulse width, we generated tail-free 200 ps laser pulses from 10 kHz to 1 GHz, ensuring a stable single-pulse energy of 0.96 pJ. Furthermore, we employed this laser as a transmitter to realize 250 MHz Return-to-Zero On-Off Keying (RZ-OOK) signal transmission in an optical communication system, providing a reliable source and clock for high-speed, high-capacity optical time-division multiplexing communication systems.

2. Numerical Simulation and Analysis of Gain-Switched Semiconductor Lasers

Gain switching is a nonlinear transient dynamical process governed by carrier–photon interactions. To quantitatively analyze the influence of the pump current on the optical output, the carrier rate equations are adopted, as described in Refs. [10,11].

$$\frac{\partial N}{\partial t} = \frac{I}{\mathrm{qV}} - v_g g S - \frac{N}{\tau_r} \tag{1}$$

$$\frac{\partial S}{\partial t} = \Gamma v_g g S - \frac{S}{\tau_p} + \Gamma \beta \frac{N}{\tau_r} \tag{2}$$

where N and S denote the carrier density and photon density, respectively. I (tens of milliamperes) is the injected current, V (typically ~10^{-17} m^3) is the active region volume, and q is the electronic charge. v_g represents the group velocity, g is the material gain, and τ_r represents the average carrier lifetime (nanoseconds). The three terms on the right-hand side of Equation (1) represent the change in minority carrier density caused by injection, stimulated recombination, and spontaneous recombination, respectively. Γ denotes the optical confinement factor, τ_p is the photon lifetime (picoseconds), and β is the spontaneous emission coupling factor (~10^{-4}). The three terms on the right-hand side of Equation (2) correspond to stimulated emission, natural photon decay, and spontaneous emission, respectively. The optical confinement factor Γ represents the fraction of photons confined within the active region, which is requisite to satisfy the oscillation conditions of the resonant cavity. The first term accounts for the accumulation of photons due to stimulated emission. The second term is generally influenced by material absorption, scattering, and reflection losses within the cavity, with typical photon lifetimes being on the order of picoseconds. The third term represents photons originating from spontaneous emission. The rate equations of the semiconductor laser are solved numerically to investigate the impact of external electrical signals on the output optical characteristics of the gain-switched semiconductor laser. In this paper, we carried out the simulation based on a 1550 nm distributed feedback laser diode. A comprehensive list of the parameters used is provided in Table 2.

Table 2. Simulation Parameters of 1550 nm Distributed Feedback (DFB) Laser Diode.

Parameter	Symbol	Value
Active region volume [10]	V	3×10^{-17} m^3
Group velocity [17]	v_g	7.5×10^7 m/s
Differential gain [18]	g	1×10^{-19} m^2
Optical confinement factor [18]	Γ	0.3
Carrier lifetime [19]	τ_r	3×10^{-9} s
Photon lifetime [20]	τ_p	5×10^{-12} s
Spontaneous emission coupling factor [10]	β	1×10^{-4}
Transparency carrier density [18]	N_t	1.2×10^{24} m^{-3}

2.1. Transient Response Analysis Under Pump Currents with Varying Repetition Frequencies

To investigate the influence of the pump current's repetition frequencies on the transient characteristics of the gain-switched laser, numerical simulations based on Equations (1) and (2) were conducted using a Gaussian pulse waveform. The specific simulation parameters are listed in Table 2. The full width at half maximum (FWHM) of the pump current was set to 200 ps, the amplitude to 40 mA, and the DC bias to 8 mA. The temporal evolutions of the carrier and photon populations were calculated at repetition rates of 100 MHz, 500 MHz, and 1 GHz, with the results presented in Figure 1. Upon the

arrival of the pump current signal, the carrier population rises sharply. Once the carrier density exceeds the stimulated emission threshold (Nth), a massive generation of photons occurs. This rapid stimulated emission heavily depletes the carriers, causing their density to drop below Nth and temporarily halting photon generation. However, since the current injection is still ongoing, the carrier density recovers to the level beyond Nth, triggering secondary photon emission. This cyclic process manifests as the tailing phenomenon trailing the primary optical pulse.

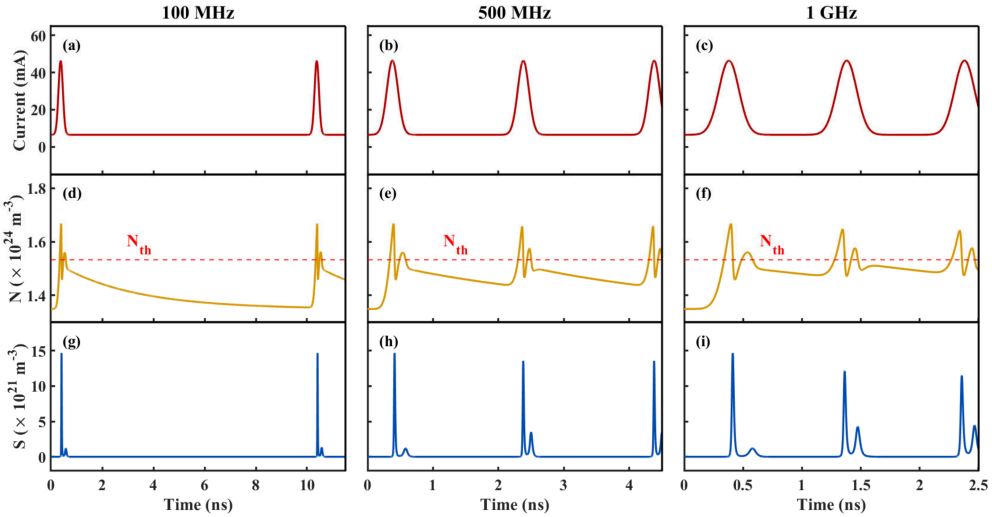

Figure 1. (**a**–**c**) Gaussian pump current waveforms at repetition frequencies of 100 MHz, 500 MHz, and 1 GHz. (**d**–**f**) Dynamics of carrier density N, where the dashed lines mark the stimulated emission threshold Nth. (**g**–**i**) Dynamics of photon density S.

Figure 1g–i depict the photon population dynamics which directly correspond to the output optical pulse waveforms. As can be seen from the figure, increasing the repetition rate leads to amplitude fluctuations across individual optical pulses, accompanied by pronounced tailing. This behavior is intrinsically linked to the carrier lifetime (τ_r = 3 ns). At a repetition rate of 100 MHz, the electrical pulse period (10 ns) exceeds the carrier lifetime. This allows the carriers injected during the preceding cycle sufficient time to fully decay via spontaneous emission and non-radiative recombination. Consequently, each optical pulse builds up from a consistent initial carrier density, yielding a stable single-pulse profile. Conversely, when the repetition rate is increased to 500 MHz, the electrical pulse interval (2 ns) becomes shorter than the carrier lifetime. Carriers injected in the previous cycle cannot completely recombine within this brief window, leading to carrier accumulation. This results in subsequent optical pulses building up from an elevated baseline carrier density, thereby inducing temporal and amplitude fluctuations in the output. In addition, a comparison between Figure 1h,i allows us to infer that the higher the repetition frequency of the pump current, the more obvious the tailing phenomenon becomes.

To address the pulse tailing phenomenon under high-frequency modulation, theoretically, the duration of the injection current can be shortened to truncate the optical pulse before the tailing occurs. However, if the electrical pulse width is too narrow, the carrier density may fail to reach the threshold or accumulate sufficiently, resulting in a sharp drop in photon density and a decrease in the peak power of the output optical pulse. Consequently, we performed a simulation analysis investigating various electrical pump pulse widths, offering a theoretical foundation for the future design of the driver circuit.

2.2. Transient Response Analysis Under Pump Currents with Varying Durations

To investigate the dynamic characteristics of optical pulses under varying injection durations, the width of the Gaussian pulse signal was incrementally reduced from 200 ps to 50 ps, as shown in Figure 2a. As the pulse width is progressively reduced from 200 ps to 150 ps, the trailing signal disappears. A further reduction to 100 ps results in a significant decrease in the photon peak. Finally, at 50 ps, the photon peak vanishes entirely, indicating that no optical pulse is generated. From Figure 2b, we can find out that the excitation time is too short for the carrier density to reach the stimulated emission threshold at the pulse width of 50 ps.

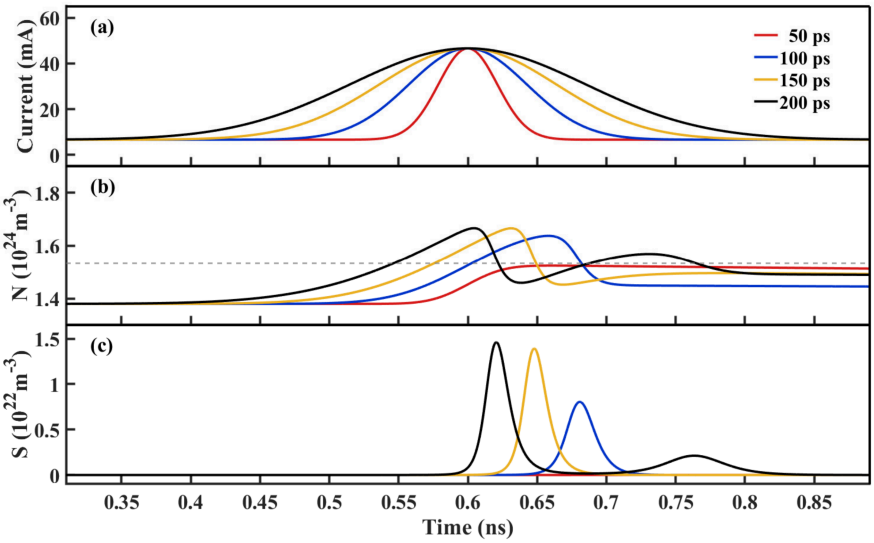

Figure 2. (**a**) Gaussian pump current waveforms with pulse widths of 50 ps, 100 ps, 150 ps, and 200 ps. (**b**) Temporal evolution of the carrier density N, where the dashed line marks, the stimulated emission threshold. (**c**) Corresponding photon density S profiles.

To compensate for the peak power attenuation caused by the reduced injection time, the amplitude or DC bias of the pump current can be appropriately increased within the tail-free pulse width regime. This approach replenishes the carrier density in the active region, enabling the elimination of tails while simultaneously boosting peak power. Consequently, stable peak power and distortion-free waveforms can be maintained across different repetition frequencies. Therefore, we propose a driving circuit capable of synergistically optimizing and fine-tuning both the current amplitude and pulse width for gain-switched laser diodes.

3. Design and Characteristics of the Driving Circuit Capable of Hybrid Current-Pulse-Width Control

Figure 3a illustrates the schematic setup of the driving circuit for gain-switched laser diodes. To achieve precise control of the pulse width and magnitude of the pump currents over a wide range of repetition rates, we demonstrate a digital relative delay method combined with a high-precision current control scheme. When the external clock signal passes through the high-speed clock fan-out buffer, it generates multiple differential signals with consistent phase and amplitude. The buffer not only provides high-drive-capability clock signals for subsequent circuits but also implements critical signal isolation, preventing the subsequent load from interfering with the stability of the preceding clock source. Subsequently, two of the differential signals are fed into a dual-channel programmable delay chip (SY89297, Microchip Technology, Chandler, AZ, USA). The FPGA independently sets the delay values for the two channels (with 5-picosecond precision) to t and (t + Δt) via

an SPI interface. The two delayed signals, now with a fixed delay difference, are sent to a high-speed logic gate for an "AND" operation, thereby generating a narrow pulse with a width of Δt at the output.

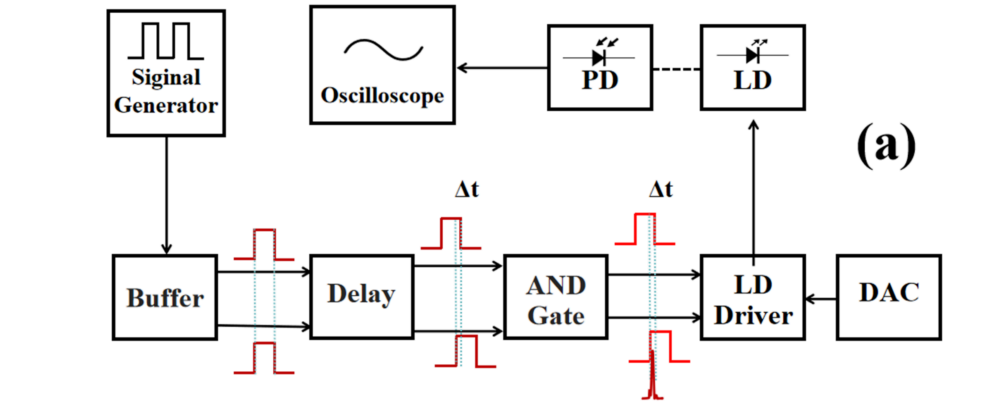

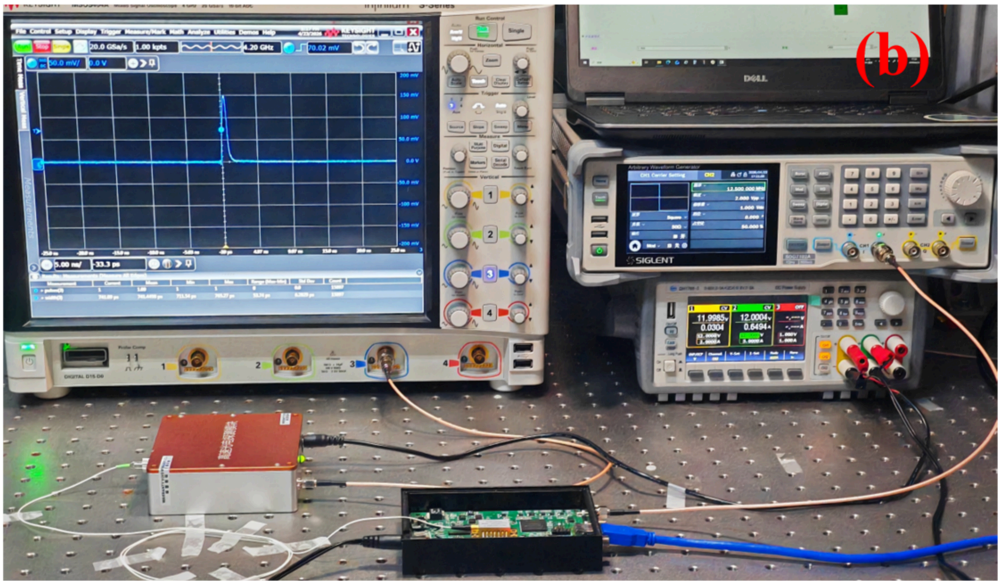

Figure 3. (**a**) Schematic setup of the driving circuit for gain-switched laser diodes. (**b**) Hardware implementation of the performance test setup for the driver module.

To achieve high-resolution regulation of the drive current, a hardware architecture integrating an FPGA, a 16-bit precision digital-to-analog converter (DAC), and a dedicated driver module has been implemented. Regarding current regulation, target current values are digitized by the FPGA and subsequently transmitted to the DAC via a high-speed SPI bus. To ensure superior linearity and stability, a low-noise precision linear regulator provides a stable 2.5 V reference voltage for the DAC. Given the 16-bit quantization level, the theoretical least significant bit (LSB) increment of the output voltage is approximately 38.15 μV. This analog signal is then fed into the control terminal of the driver module and processed by its internal voltage-to-current (V-I) conversion stage (with a conversion coefficient of ~0.09 mA/V), resulting in a fine current control precision of 3.43 μA. This configuration ensures that the system can perform precise linear adjustment of the drive current amplitude during optical pulse modulation.

This design achieves independent digital control of the pulse width and magnitude, providing hardware assurance for generating stable and reliable optical pulses at different repetition rates. To rigorously evaluate the performance of the proposed driving circuit,

we utilize a 1550 nm DFB laser diode and measure its output laser pulses, as illustrated in Figure 3b. The signal generator (SDG7012A, SIGLENT, Shenzhen, China) provides the master clock trigger, while laser output is detected by a 40-GHz photodetector (PD). The output of the PD is connected to a high-bandwidth oscilloscope (MSOS404A, Keysight, Santa Rosa, CA, USA). In addition, the integration of a specialized PC-based control interface allows for the iterative refinement of pulse-shaping parameters.

Figure 4a−e present the output waveforms of the PD at various repetition frequencies. The pulse widths are measured to be ~200 ps, while the peak amplitudes are almost the same. Furthermore, no discernible frequency-dependent tailing phenomenon has been observed. For quantitative evaluation, consecutive waveforms were recorded in infinite-persistence mode at a sampling rate of 20 GSa/s. The relative amplitude fluctuation and pulse-width jitter were 1.8% and 1.4%, respectively, calculated as the standard deviations of the pulse amplitude and pulse width normalized by their corresponding mean values. Concurrently, the optical output achieves a high extinction ratio (ER) of 32.17 dB. These results confirm that the driving circuit, through the hybrid optimization of injection current amplitude and pulse duration, successfully suppresses the tailing effect triggered by the secondary accumulation of residual carriers.

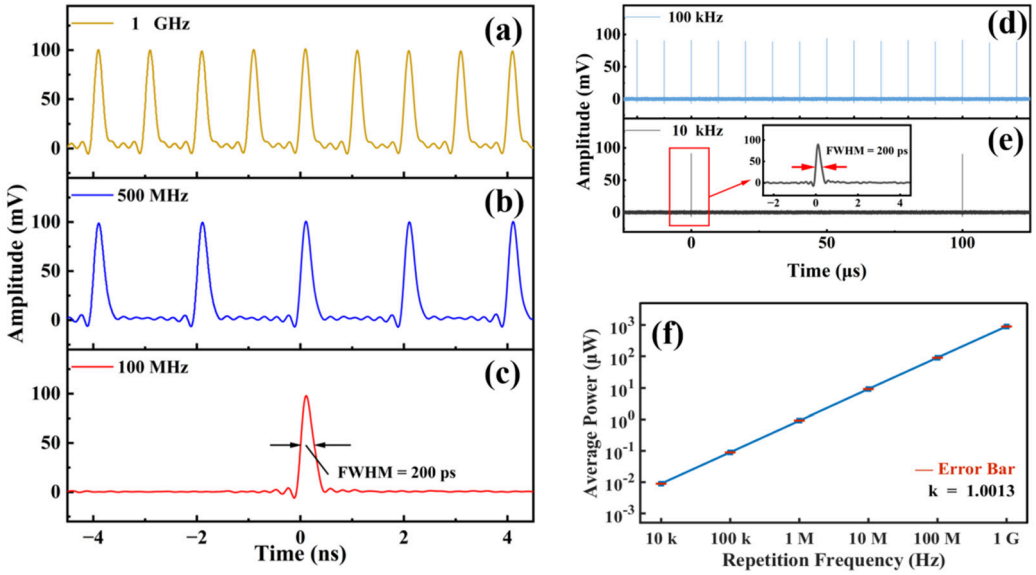

Figure 4. (**a**–**e**) Output waveforms of the PD at various repetition rates. Inset: Output waveform of the PD at 10 kHz. (**f**) Output optical power versus repetition rate (10 kHz to 1 GHz).

To evaluate the output characteristics of the laser diode over a wider range, the repetition frequency of the pump current was gradually increased from 10 kHz to 1 GHz, and the average output power was measured using an optical power meter (EPM-50, EXFO), as displayed in Figure 4f. Plotted on a logarithmic scale, the data yields a linear fitting slope of 1.0013, confirming a linear scaling of the output power with the repetition frequency. The single-pulse energy could be calculated to 0.96 pJ. Such energy invariance perfectly corroborates the uniformity of the pulse shape observed in Figure 4c, providing further validation that the pulse tailing has been well suppressed. Moreover, the peak wavelength of the laser was measured to be 1548.4 nm, while the side-mode suppression ratio (SMSR) reached 41.94 dB, verifying the high spectral purity and stable single-longitudinal-mode operation of the device. The comprehensive performance metrics confirm that the proposed laser architecture is highly capable of meeting the stringent requirements of high-speed optical communication applications.

4. Communication Verification and Discussion

We used the gain-switched 1550 nm laser to conduct the experimental coding and transmission for optical communications. The laser output was fixed at a pulse width of 200 ps, and signal modulation was implemented via the RZ-OOK format. Each time slot was set to 4 ns (corresponding to a 250 MHz frequency). The signal frame structure consisted of a 5-bit Barker code preamble, a 3-bit guard interval, and a 32-bit binary data payload. The computer-encoded electrical signal was delivered by a signal source and split into two paths using a power splitter. One path was routed directly to an oscilloscope as a reference, while the other served as the driving signal for the laser driver circuit to trigger the optical pulses. The resulting optical output was converted back into an electrical signal by the PD and captured by the oscilloscope.

As depicted in Figure 5a, a transmission latency of approximately 15 ns was observed in the received optical signal relative to the electrical reference, primarily arising from the fiber link propagation delay and the PD response time. We measured the eye diagram for the 250 MHz RZ-OOK signal, as shown in Figure 5b. The experimental results exhibit a clear and wide-open eye pattern, indicating a high Signal-to-Noise Ratio (SNR). It should be noted that the minor fluctuations and undershoot observed at the logic '0' level are intrinsic to the transient response of the photo detector (PD) used for detection. The experimental results verify that the output signal of the laser can be accurately demodulated and recovered to the original data. Moreover, 200 ps optical pulses generated from higher-repetition-rate current pulses are intrinsically capable of enabling optical transmission at substantially increased data rates.

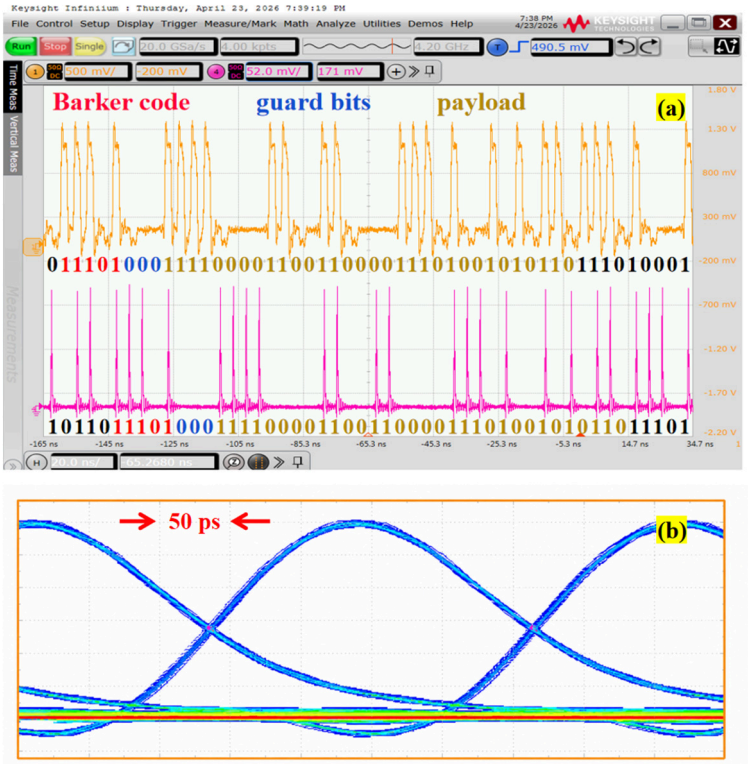

Figure 5. (**a**) Comparison of RZ-OOK modulated electrical driving signal and emitted optical signal. (**b**) Measured eye diagram of the 250-MHz RZ-OOK signal.

5. Conclusions

In conclusion, this work addresses the challenge of relaxation oscillations and pulse tailing in gain-switched semiconductor lasers for high-speed applications. A transient dynamics model based on rate equations was established, revealing that at high repetition

rates, pulse tailing arises when the carrier recovery time exceeds the electrical pulse period. To suppress this effect, we designed a high-precision driving circuit capable of digitally adjusting the current amplitude (with ~3 μA precision) and pulse width (with 5 ps resolution). Utilizing this circuit to drive a commercial 1550 nm DFB laser, we successfully generated tail-free optical pulses with a duration of 200 ps across a repetition rate range of 10 kHz to 1 GHz. These results indicate that this approach enables narrow-pulse laser generation with high integration and broad repetition-rate tunability. The feasibility of the proposed solution was validated by employing the laser as a transmitter for 250 MHz RZ-OOK signal transmission. This work thus provides a stable and versatile high-speed optical source for applications in high-speed optical communications and laser ranging.

Author Contributions: Methodology, Y.L.; investigation, Y.Q.; validation, J.F.; writing—original draft preparation, J.F.; writing—review and editing, Y.L.; Supervision and Funding acquisition, H.Z. All authors have read and agreed to the published version of the manuscript.

Funding: This work was supported by Shanghai Municipal Science and Technology Major Project (2019SHZDZX01), the Innovation Program for Quantum Science and Technology (2023ZD0301000), and the National Natural Science Foundation of China (62175152).

Institutional Review Board Statement: Not applicable.

Informed Consent Statement: Not applicable.

Data Availability Statement: Data underlying the results presented in this paper are not publicly available at this time but may be obtained from the authors upon reasonable request.

Conflicts of Interest: The authors declare no conflicts of interest.

Abbreviations

The following abbreviations are used in this manuscript:

DFB	Distributed Feedback
FWHM	Full width at half maximum
DAC	Digital-to-analog converter
LSB	Least significant bit
PD	Photodetector
ER	Extinction ratio
SMSR	Side-mode suppression ratio
RZ-OOK	Return-to-Zero On-Off Keying

References

1. Hao, H.; Zhao, Q.; Huang, Y.; Deng, J.; Yang, F.; Ru, S.; Liu, Z.; Wan, C.; Liu, H.; Li, Z.; et al. A compact multi-pixel superconducting nanowire single-photon detector array supporting gigabit space-to-ground communications. *Light Sci. Appl.* **2024**, *13*, 25. [CrossRef] [PubMed]
2. Shafi, K.M.; Chawla, P.; Hegde, A.S.; Gayatri, R.S.; Padhye, A.; Chandrashekar, C.M. Multi-bit quantum random number generator from path-entangled single photons. *EPJ Quantum Technol.* **2023**, *10*, 43. [CrossRef]
3. Le Roy-Deloison, T.; Lobo, E.; Pauwels, J.; Pironio, S. Device-independent quantum key distribution based on routed Bell tests. *PRX Quantum* **2025**, *6*, 010313. [CrossRef]
4. Tsay, H.-L.; Chang, C.-H.; Lin, F.-Y. Random-modulated pulse lidar using a gain-switched semiconductor laser with a delayed self-homodyne interferometer. *Opt. Express* **2023**, *31*, 2013–2028. [CrossRef] [PubMed]
5. Zeng, L.; Liu, G.; Yang, D.; Ji, X. 3D-visual laser-diode-based photoacoustic imaging. *Opt. Express* **2012**, *20*, 1237–1246. [CrossRef] [PubMed]
6. Comandar, L.C.; Lucamarini, M.; Fröhlich, B.; Dynes, J.F.; Yuan, Z.L.; Shields, A.J. Near perfect mode overlap between independently seeded, gain-switched lasers. *Opt. Express* **2016**, *24*, 17849–17859. [CrossRef] [PubMed]
7. Quevedo-Galán, C.; Durán, V.; Rosado, A.; Pérez-Serrano, A.; Tijero, J.M.G.; Esquivias, I. Gain-switched semiconductor lasers with pulsed excitation and optical injection for dual-comb spectroscopy. *Opt. Express* **2020**, *28*, 33307–33317. [CrossRef] [PubMed]

8. Anandarajah, P.M.; Clarke, A.M.; Guignard, C.; Bramerie, L.; Barry, L.P.; Harvey, J.D.; Simon, J.C. System-performance analysis of optimized gain-switched pulse source employed in 40- and 80-Gb/s OTDM systems. *J. Light. Technol.* **2007**, *25*, 1495–1503. [CrossRef]
9. Grigoryan, V.S.; Carter, G.M.; Menyuk, C.R. Tolerance of dispersion-managed soliton transmission to the shape of the input pulses. *IEEE Photon. Technol. Lett.* **2000**, *12*, 1165–1167. [CrossRef]
10. Lovic, V.; Marangon, D.G.; Lucamarini, M.; Yuan, Z.; Shields, A.J. Characterizing phase noise in a gain-switched laser diode for quantum random-number generation. *Phys. Rev. Appl.* **2021**, *16*, 054012. [CrossRef]
11. Yang, Z.; Wu, X.; Ouyang, D.; Zhang, E.; Sun, H.; Ruan, S. Pulse control of frequency and width for a real-time independently adjustable laser source. *Front. Inf. Technol. Electron. Eng.* **2021**, *22*, 1379–1389. [CrossRef]
12. Xia, M.; Ghafouri-Shiraz, H.; Hou, L.; Kelly, A.E. High-speed pulse train amplification in semiconductor optical amplifiers with optimized bias current. *Appl. Opt.* **2017**, *56*, 1079–1086. [CrossRef]
13. Yang, J.; Chen, H.; Song, S.; Chen, G.; Zhao, P. Single-frequency erbium-doped fiber laser based on self-injection feedback. *Opt. Express* **2024**, *32*, 27399–27408. [CrossRef]
14. Wada, K.; Takamatsu, S.; Watanabe, H.; Matsuyama, T.; Horinaka, H. Pulse-shaping of gain-switched pulse from multimode laser diode using fiber Sagnac interferometer. *Opt. Express* **2008**, *16*, 19872–19881. [CrossRef]
15. Li, B.; Sun, C.; Ling, Y.; Zhou, H.; Qiu, K. Step-pulse modulation of gain-switched semiconductor pulsed laser. *Appl. Sci.* **2019**, *9*, 602. [CrossRef]
16. Wang, C.; Cao, F.; Liu, Y.; Nakamae, H.; Kobayashi, M.; Jiang, D.; Qi, Y.; Weng, G.-E.; Hu, X.; Akiyama, H.; et al. Electrically smoothing gain-switched optical pulses from a semiconductor laser diode. *Opt. Lett.* **2024**, *49*, 6285–6288. [CrossRef]
17. Coldren, L.A.; Corzine, S.W.; Mashanovitch, M.L. *Diode Lasers and Photonic Integrated Circuits*, 2nd ed.; John Wiley & Sons: Hoboken, NJ, USA, 2012; pp. 98–215.
18. Agrawal, G.P.; Dutta, N.K. *Semiconductor Lasers*, 2nd ed.; Van Nostrand Reinhold: New York, NY, USA, 1993; pp. 25–62.
19. Yokouchi, N.; Yamanaka, N.; Iwai, N.; Nakahira, Y.; Kasukawa, A. Tensile-strained GaInAsP-InP quantum-well lasers emitting at 1.3 μm. *IEEE J. Quantum Electron.* **1996**, *32*, 2148–2155. [CrossRef]
20. Cartledge, J.C.; Burley, G.S. The effect of laser chirping on lightwave system performance. *J. Light. Technol.* **1989**, *7*, 568–573. [CrossRef]

Disclaimer/Publisher's Note: The statements, opinions and data contained in all publications are solely those of the individual author(s) and contributor(s) and not of MDPI and/or the editor(s). MDPI and/or the editor(s) disclaim responsibility for any injury to people or property resulting from any ideas, methods, instructions or products referred to in the content.